ELSEVIER

Surface Science 453 (2000) 25–31

surface science

www.elsevier.nl/locate/susc

Adsorption and energetics of isolated CO molecules on Pd(111)

P. Sautet [a,b], M.K. Rose [c,1], J.C. Dunphy [c,2], S. Behler [c,3], M. Salmeron [c,*]

[a] *Laboratoire de Chimie Thèorique, Ecole Normale Superieure, 69364 Lyon Cedex 07, France*
[b] *Institut de Recherche sur la Catalyse, CNRS, 69626 Villeurbanne Cedex, France*
[c] *Materials Sciences Division, Lawrence Berkeley National Laboratory, University of California, Berkeley, CA 94720, USA*

Received 18 October 1999; accepted for publication 11 January 2000

Abstract

The adsorption of CO on Pd(111) has been studied with scanning tunneling microscopy in the very low coverage regime. Isolated CO molecules were imaged with two different corrugations of ~ 0.25 Å and ~ 0.15 Å, which are attributed to adsorption of the hcp and fcc hollow sites. Total energy calculations reveal that these two sites are the most favorable ones. Calculated image profiles using the ESQC method agree well with the experimental corrugations.

Keywords: Carbon monoxide; Chemisorption; Density functional calculations; Palladium; Scanning tunneling microscopy; Semi-empirical models and model calculations; Single crystal surfaces

1. Introduction

Carbon monoxide is a widely used molecule in catalysis, both as a reactant and as a specific probe of the surface of metal catalysts. Oxidation of CO is an important environmental process and palladium has been used as a model catalyst for this reaction [1]. On the (111) face, CO displays a series of ordered structures with increasing coverage, the first one being the $(\sqrt{3}\times\sqrt{3})R30^\circ$, which is formed at 0.33 monolayer (ML) [2,3]. Below that coverage, no ordered pattern is observed by diffraction and, therefore, the structure and adsorption geometry of the molecules are unknown. In addition to diffraction studies, the CO–Pd(111) system has been studied with a variety of spectroscopic techniques [4–8]. Unsolved questions remain concerning the very low coverage limit of isolated molecules and the energy difference between various adsorption sites.

Scanning tunneling microscopy (STM), a real-space imaging technique, is ideal for these studies, since it can give information on the disordered phases, including, in particular, the limit of isolated molecules at very low coverage. No such studies of isolated CO molecules on Pd(111) have been reported yet. In this paper, we present both theoretical and experimental results on this system that fill some of these gaps. In addition to providing a test for theoretical models of chemisorption (based on total energy calculations), it also allows us to test theoretical methods of calculating STM image

* Corresponding author. Fax: +1-510-486-4995.
E-mail address: salmeron@stm.lbl.gov (M. Salmeron)
[1] Also in the Department of Physics, University of California, Berkeley, CA 94720, USA.
[2] Present address: Candescent Technologies, 6580 Via del Oro, San Jose, CA 95119, USA.
[3] Present address: ESEC SA, Hinterbergstrasse 32, CH-6330 Cham, Switzerland.

0039-6028/00/$ - see front matter
PII: S0039-6028(00)00243-0

contrast, which require knowledge of the geometry of the adsorbate.

2. Experimental

The STM experiments were conducted in an ultrahigh vacuum (UHV) chamber equipped with a continuous-flow liquid helium cryostat for sample cooling. Low temperature operation is essential to stabilize low coverage molecular structures, because of the high mobility of isolated molecules. Details of the apparatus are published elsewhere and will not be discussed here [9]. The STM tip is an electrochemically etched Pt–Rh(10%) wire conditioned in vacuum by field emission to an auxiliary tungsten electrode.

The Pd(111) sample was cleaned by cycles of Ar^+ ion sputtering followed by heating in oxygen. No impurities could be detected by Auger spectroscopy. Immediately after the final cycle, the sample was cooled to 25 K and imaged by STM. Not surprisingly, STM images were found to provide the most reliable and stringent test of surface cleanliness, since an impurity atom in an area of $\sim 100 \times 100$ atoms is easily visible. After obtaining a clean surface (impurity level below 0.01% of a monolayer), CO was adsorbed by exposure to gas leaked into the UHV chamber.

3. Total energy calculations

The optimal structure of the CO ad-layer was determined by minimization of the total energy, calculated using density functional theory (DFT). Most of the results have appeared in a previous paper, and we will only recall the major points here [10]. The system is modeled by a four-layer slab of Pd atoms, with surfaces of (111) orientation. The top surface is covered with a periodic layer of chemisorbed CO. A $(\sqrt{3} \times \sqrt{3})$R30°–1CO structure was considered, which corresponds to a coverage of 0.33 ML. The two uppermost Pd layers and the CO molecule were included in the optimization of the geometry.

The DFT calculations were performed with the Vienna ab initio simulation program (VASP) [11–13]. The Kohn–Sham equations were solved on a basis set of plane waves, with the generalized gradient approximation (GGA) proposed by Perdew et al. for the exchange and correlation potential [14]. Ultrasoft pseudopotentials are used to describe the electron–ion interactions, which makes possible a truncation of the plane-wave expansion at an energy of 400 eV. Convergence with the number of $\boldsymbol{k}$-points in the two-dimensional Brillouin zone has been checked.

4. Theoretical simulation of STM images

Theoretical simulations of STM images were performed using the optimized geometry obtained from the total energy calculations. The method to calculate the tunnel current has been described in previous papers [15]. It considers simultaneously the sample bulk, its surface with adsorbates, the tip apex and the tip bulk. The tunnel current is calculated at low bias voltage from the electronic scattering matrix. This matrix contains the electronic transmission probabilities at the tunnel junction for electrons traveling in propagative channels on the sample and tip. For the propagative procedure, the Hamiltonian is projected on a Slater-type atomic basis set. Overlap matrix elements are calculated between the atomic basis functions, and the Hamiltonian matrix elements are obtained using the extended Hückel approximation. For the STM calculations, a (4×4) surface unit cell is used with periodic boundary conditions. A Pd bulk structure has been considered for the sample and tip. The basis set was limited to 5s orbitals for the bulk atoms (neglect of d orbitals in the bulk has been justified in several examples). However, a full spd basis set was used in the tunnel gap regions for the two uppermost surface layers and for the tetrahedral 4Pd tip apex. One CO molecule is positioned on the (4×4) unit cell. In order to describe the long-range interactions between the tip and surface better, all the atoms in the tunnel gap region are described by a double zeta valence basis set, with exponents determined by Hartree–Fock calculations [16].

5. Experimental results

The sample was held at 25 K and exposed to 1×10^{-9} Torr for 60 s. An example of an STM image obtained after dosing is shown in Fig. 1a. Isolated CO molecules appear as small bumps surrounded by shallow depressions. The depressions are approximately 0.1 Å deep and 6 Å in diameter. Although the measured corrugations vary slightly with tunneling conditions, two types of bumps with different heights are apparent in the topographic (constant current) images. The high corrugation CO molecule rises $\sim$0.25 Å above the Pd surface, and the low corrugation one rises only $\sim$0.15 Å.

Although the images were obtained under conditions of minimal tip perturbation, we could also observe tip-induced displacement of molecules over several distinct tunneling regimes. One is at high bias voltage (>500 mV) and the other at high tunnel currents (≥ 1 nA), both of which point to electronic excitations caused by the tunneling electrons [17]. Another perturbation occurs when imaging at low gap resistance (<200 MΩ), which suggests a more direct or 'chemical' interaction of the CO with the tip.

Very low gap resistance imaging, below 1 MΩ, was found to be necessary to resolve the Pd lattice. At such low gaps, any CO initially present is swept aside by the STM tip. Therefore, we could not resolve both the CO molecules and the atomic lattice of the substrate in the same image. Also, owing to thermal drift, it was not possible to determine the registry between the CO and the Pd lattice through comparison of images acquired at high and low gap resistance. However, by manually overlaying the high gap image onto the low gap image, various registry models could be explored.

With this procedure, we find that, after placing one CO molecule on a given Pd site, all similarly corrugated CO molecules fall on sites of the exact same symmetry. Similarly, all CO molecules of the other corrugation fall on a different, but unique symmetry site. We thus conclude that the corrugation difference in the STM images is due to the local adsorption sites of the CO molecules. Restricting the choice to the highest symmetry sites, it is easily seen that only three registries are

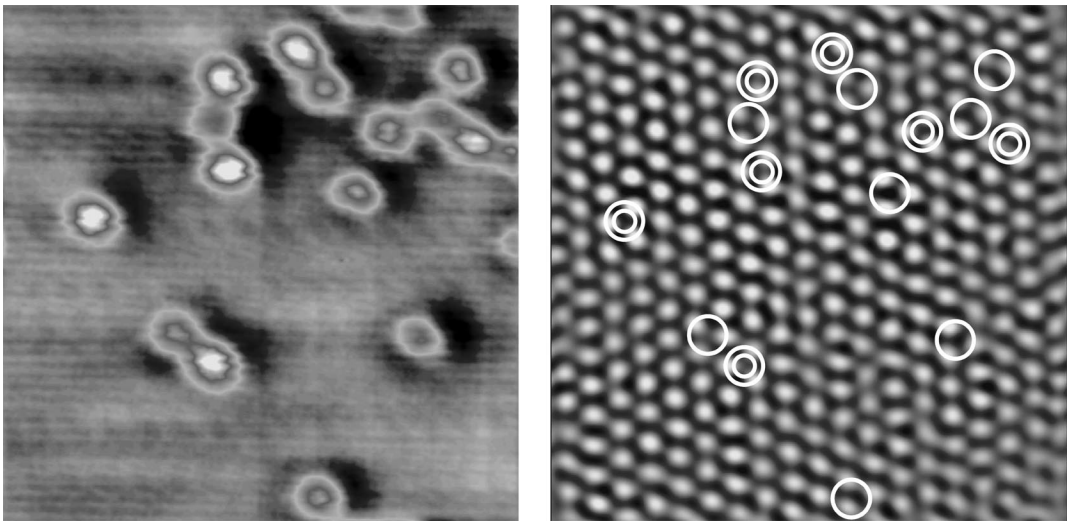

Fig. 1. (a) (left) 45×45 Å^2 STM image of a Pd(111) surface with low coverage of CO acquired at 25 K. Protrusions with two different heights (0.15 and 0.25 Å) are observed. The protrusions are surrounded by depressions. Tunneling conditions are 50 mV bias voltage and 0.1 nA tunnel current. (b) (right) 45×45 Å^2 STM image of the same area at lower gap resistance. The underlying Pd lattice is now resolved (the CO molecules are displaced by the tip and cannot be imaged under the conditions of 10 mV bias, 17 nA tunnel current). The single and double circles correspond to the low and high CO protrusions in (a), which are superimposed on the image. Only one of three high symmetry adsorption models is shown.

possible, which involve only top and threefold hollow sites. A model in which one CO molecule sits on a top site was presented in an earlier paper [9]. Fig. 1b shows an STM image of the Pd lattice obtained at low gap immediately after acquisition of the image in Fig. 1a. The circles in Fig. 1b correspond to each of the CO bumps in the high gap image in Fig. 1a. We overlaid them such that all bumps occupy threefold hollow sites, both hcp and fcc. However, we have no independent way to distinguish these two sites. The other two high symmetry registries (not shown) involve a top and a threefold hollow site.

6. Theory results

The system was modeled by a $(\sqrt{3}\times\sqrt{3})$R30°–1CO structure (0.33 ML) on the slab. Although this coverage is much higher than that for the isolated molecules in the STM experiment, we will assume that molecule–molecule interactions are small enough that the relative energies between sites and the adsorbate geometry can be transferred to the very low coverage cases. Several sites for CO have been considered and the results are summarized in Fig. 2. Clearly the most stable sites are the hollow sites, with only a small energy difference (0.03 eV) between the fcc and the hcp cases. The bridge site is found to be 0.2 eV higher in energy than the most stable fcc hollow site. It corresponds to a saddle point between the two hollow local minima. The top site is a local maximum on the potential energy surface, and is 0.65 eV higher than the fcc hollow. The total energy calculation therefore leads us to interpret the STM image as corresponding to a mixture of fcc and hcp hollow sites. The 0.2 eV energy barrier is consistent with other measurements [18,19] and with an estimate based on the temperature at which the molecules become mobile, as seen in the STM images.

Table 1
Calculated carbon (z_C) and oxygen (z_O) heights above the surface for the $(\sqrt{3}\times\sqrt{3})$R30° CO structure on Pd(111)

	z_C (Å)	z_O (Å)
fcc hollow	1.296	2.485
hcp hollow	1.300	2.488
Bridge	1.42	2.60
Top	1.87	3.03

The z coordinates of C and O with respect to the Pd surface are given in Table 1. There is clearly a very small difference for these z values between the fcc and hcp hollow sites (0.004 Å). A test calculation performed on a lower coverage (2×2) structure (0.25 ML) shows only small changes in the C and O optimal coordinates (less than 0.01 Å). Therefore, a higher or longer CO molecule on one site compared with the other cannot explain the contrast difference observed for the two types

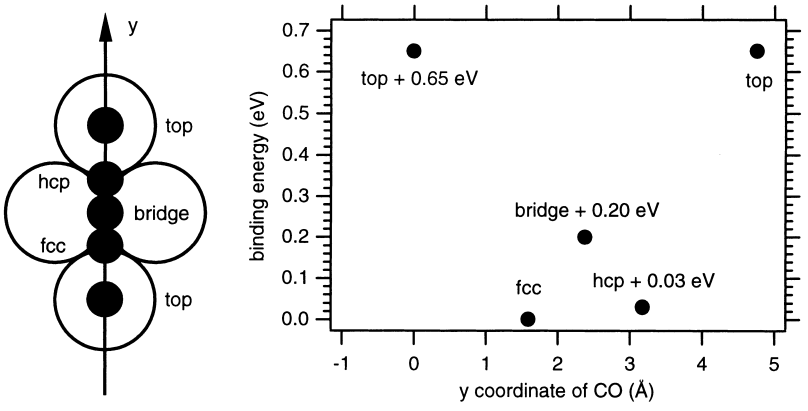

Fig. 2. Calculated total energy as a function of binding site for a $(\sqrt{3}\times\sqrt{3})$R30° structure of CO on a Pd(111) surface. All energies are relative to the most stable case: the fcc hollow site.

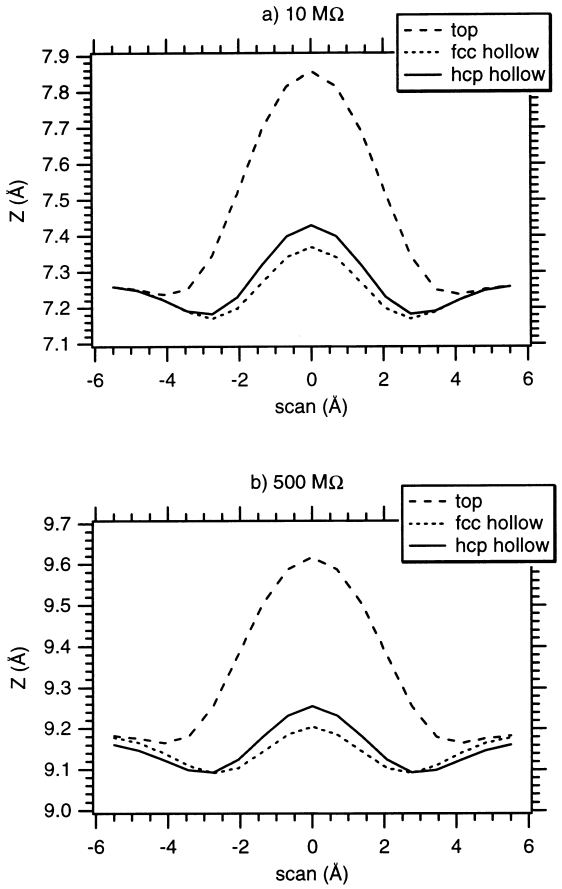

Fig. 3. Calculated STM topographic scan lines across the CO molecule for the hollow sites and the top site. Tunneling gap resistances of (a) 10 MΩ, and (b) 500 MΩ are used.

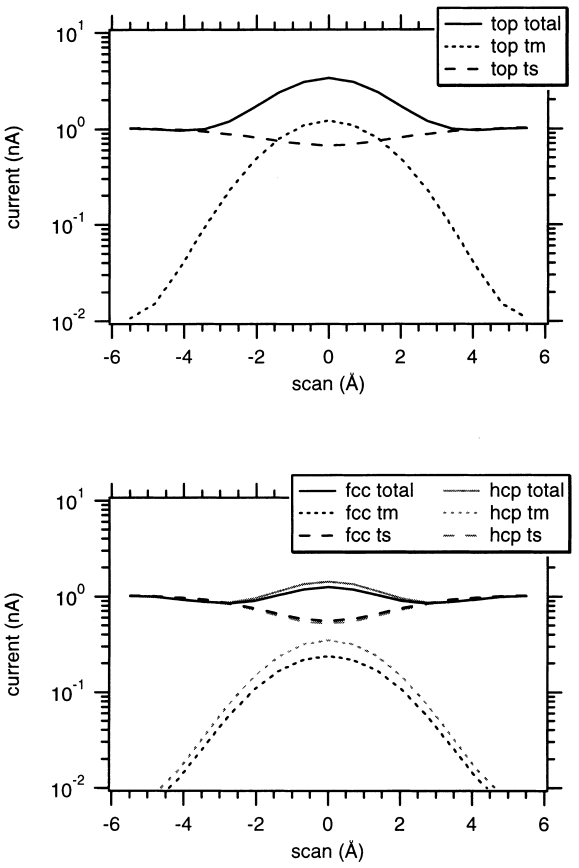

Fig. 4. STM current analysis for CO: (a) (top) on the top site, and (b) (bottom) on the fcc hollow site and hcp hollow site. Total current (solid line), through molecule current (tm, dotted line) and through surface current (ts, dashed line) are given.

of CO sites. This should instead be related to a more subtle electronic effect.

Simulated STM scans are given in Fig. 3 for the high symmetry sites: top, fcc and hcp. The top site produces a bump with a height of 0.43 Å (for a 500 MΩ resistance), whereas much smaller maxima are produced in the cases of the two hollow sites. A similar trend was found for CO on Pt(111) [20]. The height differences are mainly related to the higher z coordinate of the top molecule (closer to the tip). These results exclude the existence of top site molecules at low coverage. The calculated corrugations for the hcp and fcc sites at 500 MΩ are 0.16 Å and 0.11 Å respectively, which compare favorably with the slightly larger values of 0.25 Å and 0.15 Å found experimentally. On that basis, we can conclude that, at low coverage, these are the sites populated by the adsorbed CO molecules.

The calculation predicts a significantly higher STM contrast for the hcp CO than for the fcc CO, despite their very similar geometry. This singular behavior can be understood by the following analysis of the origin of the tunnel current. In a first step, the tunnel current can be decomposed into tunneling contributions through the molecule and through the surface. Plots of the tunnel current and of these two contributions as the tip scans at constant height are shown in Fig. 4. Similar to the case of CO on Pt(111), the 'through surface' current decreases in the vicinity of the molecule. Although

the effect is always present, it is larger for the multiple coordinated sites where several Pd atoms are perturbed by the CO adsorption. There is very little difference between the hollow sites, so the fcc–hcp difference does not arise from a different adsorbate-induced perturbation of the surface. The 'through molecule' contribution is largest when the tip is on top of the molecule and, for a given tip–surface distance, it is much larger for the top site, mainly because the molecule is closer to the tip. For the hcp hollow site, the 'through molecule' current is 1.5 times larger than for the fcc hollow site, despite their identical z coordinates. So the difference between the hollow sites lies entirely in the through molecule component.

To understand this difference, we further decompose the 'through molecule' current into contributions of the CO molecular orbitals (MOs). The contributions of the most important orbitals are given in Fig. 5a for the top site and in Fig. 5b for the hcp and fcc sites. Independent of the binding site, the 5σ orbital of CO contributes the most to the tunnel current. This orbital is close to the Fermi level and has a favorable interaction with the surface and the tip. The second contribution arises from the 3σ orbital, which is lower in energy. The π orbitals of CO give a very small current contribution, because they are not correctly oriented to interact favorably with the tip apex (they have a vertical nodal plane at the position of the molecule).

If one now considers the total tunnel current (solid lines in Fig. 5), a very surprising feature is that it is almost an order of magnitude lower than the largest MO contribution. This comes from the strong destructive interference between the 5σ and 3σ contributions. The wave functions of the 5σ and the 3σ MOs of CO at the Fermi level have opposite phase and, therefore, when one has a positive overlap with the tip, the second one has a negative one. If we now again compare the fcc and the hcp hollow sites, the MO contributions are very similar (the hcp components are only slightly larger) and most of the 1.5 factor arises from a different amplitude of the destructive interference, which is more pronounced for the fcc site. The amplitude of the destructive interference is controlled by the small weight of the 3σ CO orbital at the Fermi level, which can be modified by subtle variations of the binding site.

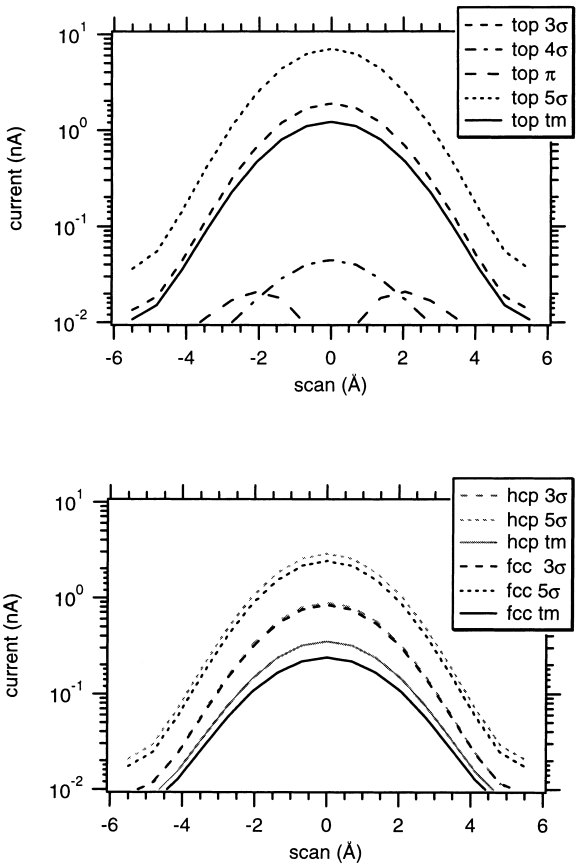

Fig. 5. Decomposition of the through molecule current (tm) in contributions of CO MOs: (a) (top) for the top site CO, and (b) (bottom) for the fcc and hcp hollow site CO.

7. Conclusions

We have shown that, at low coverage, CO molecules adsorb with almost similar probability on two different sites of the Pd(111) surface. From the STM images alone, possible pairs of sites include top–hollow (fcc or hcp) and hcp–fcc hollow sites. In the images, CO appeared as protrusions of 0.25 and 0.15 Å (at 50 mV bias and 0.1 nA tunnel current), surrounded by a shallow depression (∼0.1 Å).

Total energy calculations indicate that the most favorable sites are the two threefold hollow sites, with only a small energy difference (0.03 eV) between them. Using the theoretically determined adsorption geometry, the shape of the STM images

was obtained using the ESQC method. The simulated images for CO on these two sites are in reasonable agreement with the experimental images both in the corrugations (0.16 and 0.11 Å) and surrounding depression. In contrast, images calculated for top sites show considerably higher corrugation. The different CO corrugations in the hcp and fcc sites are due to electronic interference effects between contributions of different CO MOs.

Acknowledgements

This work was supported by the Director, Office of Science, Office of Basic Energy Sciences, Division of Materials Sciences under US Department of Energy Contract No. DE-AC03-76SF00098. P.S. thanks IDRIS (Project 980016) for contribution of CPU time.

References

[1] T. Engel, G. Ertl, Adv. Catal. 28 (1979) 1.
[2] J.P. Biberian, M.A. Van Hove, Surf. Sci. 138 (1984) 361.
[3] H. Ohtani, M.A. Van Hove, G.A. Somorjai, Surf. Sci. 187 (1987) 372.
[4] A.M. Bradshaw, F.M. Hoffman, Surf. Sci. 72 (1978) 513.
[5] P.D. Johnson, S.L. Hulbert, Phys. Rev. B 35 (1987) 9427.
[6] H. Conrad, G. Ertl, J. Koch, E.E. Latta, Surf. Sci. 43 (1974) 462.
[7] F.M. Hoffmann, Surf. Sci. Rep. 3 (1983) 107.
[8] K. Kuhn, J. Szanyi, D.W. Goodman, Surf. Sci. 274 (1992) L611.
[9] S. Behler, M.K. Rose, J.C. Dunphy, D.F. Ogletree, M. Salmeron, C. Chapelier, Rev. Sci. Instrum. 68 (1997) 2479.
[10] D. Loffreda, D. Simon, P. Sautet, Surf. Sci. 425 (1999) 68.
[11] G. Kresse, J. Hafner, Phys. Rev. B 49 (1994) 14 251.
[12] G. Kresse, J. Furthmuller, Phys. Rev. B 54 (1996) 11 169.
[13] G. Kresse, J. Hafner, Phys. Rev. B 47 (1993) 558.
[14] J.P. Perdew, J.A. Chevary, S.H. Vosko, K.A. Jackson, M.R. Pederson, D.J. Singh, C. Fiolhais, Phys. Rev. B 46 (1992) 6671.
[15] P. Sautet, C. Joachim, Phys. Rev. B 38 (1988) 12 238.
[16] E. Clementi, C. Roetti, At. Data Nucl. Data Tables 14 (1974) 177.
[17] L. Bartels, G. Meyer, K.H. Rieder, D. Velic, E. Knoesel, A. Hotzel, M. Wolf, G. Ertl, Phys. Rev. Lett. 80 (1998) 2004.
[18] M. Snabl, O. Borusik, V. Chab, M. Ondrejcek, W. Stenzel, H. Conrad, A.M. Bradshaw, Surf. Sci. 385 (1997) L1016.
[19] S.E. Shore, J.P. Ansermet, C.P. Slichter, J.H. Sinfelt, Phys. Rev. Lett. 58 (1987) 953.
[20] M.O. Pedersen, M.L. Bocquet, P. Sautet, E. Laegsgaard, I. Stensgaard, F. Besenbacher, Chem. Phys. Lett. 299 (1999) 403.